MSc Molecular Techniques in Life Science

Karolinska Institutet, Stockholm, Sweden

June 2022

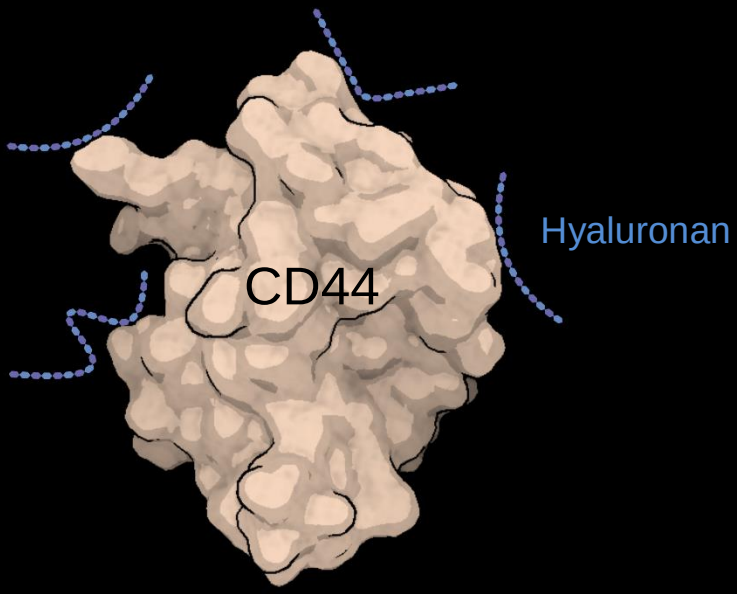

Role of the glycocalyx on the dynamics of membrane proteins

Cenk Onur Gurdap

Supervisors:

Erdinc Sezgin

Taras Sych

SciLifeLab, Karolinska Institutet

Department of Women's and children's health

CONTENTS Page numbers

LIST OF ABBREVIATIONS

Plasma membrane – PM

Membrane proteins – MPs

Extracellular domain of glycoproteins – GlyP-ECD

Cluster of differentiation – CD

Hyaluronic acids – HA

Sphingomyelin – SM

Giant unilamellar vesicles – GUVs

Fluorescence correlation spectroscopy – FCS

Histidine – His

Predicted amino acids weight – PMW_{aa}

1-palmitoyl-2-oleoyl-sn-glycero-3-phosphocholine – POPC

1,2-dioleoyl-sn-glycero-3-[(N-(5-amino-1-carboxypentyl)iminodiacetic acid)succinyl] (nickel salt) (18:1 DGS-NTA(Ni)) – DOGS NTA

Integrin alpha 5 beta 1 – Integrin

Podocalyxin – PODXL

Molecular weight – MW

Hyaluronic acid binding domain – HABD

Abberior STAR Red-1,2-Dipalmitoyl-sn-glycero-3-phosphatidylethanolamine – AbStR-DPPE

Abberior STAR Red-sphingomyelin – AbStR-SM

Alexa Fluor 488 NHS Ester – A488

Phosphate-buffered saline – PBS

Low molecular weight – LMW

High molecular weight – HMW

ABSTRACT

Most complex signaling events at the plasma membrane (PM) are driven by the lateral organization and dynamics of membrane proteins (MPs) and their interaction with other membrane-associated components such as lipids, actin cytoskeleton, and glycocalyx. Various advanced imaging tools have aided in investigating these interactions showing the variety of MPs diffusion modes, defined by constraints introduced either by cytoskeleton or extracellular matrix. Although these recent discoveries have revolutionized our understanding of the interplay between MPs and the cortical cytoskeleton for such constraints, the impact of the glycocalyx on MP dynamics is an unexplored question. Here, we investigate the biophysical determinants of the glycocalyx-protein interplay by dissecting these complex interactions in model membranes with tunable complexity and specificity. We first used fluorescence correlation spectroscopy to study the diffusion of the extracellular domain of glycoproteins (GlyP-ECD). We observed that GlyP-ECD mobility decreases as the absolute molecular weight increases due to glycosylation but is not directly correlated with the amino acids weight. We then reconstituted CD44-ECD bound to hyaluronic acids (HA) of different sizes in model membranes and analyze CD44 diffusion. We observed that increasing HA size leads to a decrease in CD44 mobility. We lastly reconstituted CD44 together with sphingomyelin (SM), both having a binding affinity for HA. CD44 could potentially create a physical barrier for HA to bind to SM, which is normally pro-inflammatory. Our data suggest a critical role of the glycocalyx components on MP dynamics in the PM and paves the way to a better understanding of the glycocalyx-protein dynamics in health and disease.

INTRODUCTION

The plasma membrane (PM) is a complex and dynamic structure continuously regulating the spatiotemporal organization of lipids, membrane proteins (MP), actin cytoskeleton, glycocalyx, extracellular matrix, and their interaction dynamics. The traditional fluid mosaic model[1] has profoundly influenced the opinions on the structure and dynamics of the PM, mainly suggesting a homogeneous system based on free Brownian motion. This model has been modernized to account for further observations, especially regarding the raft hypothesis[2] and the interactions of membrane-associated cytoskeletal components[3]. Membrane rafts explicitly expand the mosaic nature of the membrane to include functionally independent and different fluid domains, which are selective in both protein and lipid components, suggesting different molecular mobilities in segregated domains. The actin cytoskeleton, on the other hand, acts as a physical barrier to MPs and slows down their diffusion. There have been additional suggestions for the regulation of MP dynamics, such as specific protein-lipid interactions[4] and molecular crowding[5]. Thus, many MPs are not entirely in free Brownian motion in the PM, but rather their mobilities are regulated locally[6].

One of the relatively newly emerging membrane-associated components that regulates the organization and dynamics of MPs is the glycocalyx. The glycocalyx, a dense sugar coat on the cell surface, consists of free glycans, glycolipids, glycoproteins, and proteoglycans. It shows a high structural variance aiding specific molecular recognition. Therefore, it plays a key role in various cellular activities[7] including host-pathogen interactions[8], cell adhesion[9], cancer aggregation[10], and membrane topology[11]. The glycocalyx components are complex structures, assembled by one or multiple monosaccharide units building up to oligosaccharides or glycoconjugates by attaching to other molecular species[12,13]. Carbohydrates are crucial constituents of all mammalian membranes, and their synthesis and distribution on the membrane must be tightly regulated. Their synthesis takes place in different cellular compartments via various pathways[14]. For instance, while the synthesis of glycoproteins is initiated in the endoplasmic reticulum, where glycosylation of folded protein occurs and they are further modified in the Golgi apparatus, some glycocalyx components (e.g., hyaluronic acid (HA)) are directly assembled by MPs (e.g., hyaluronan synthases) at the cell surface. Although these syntheses may seem chaotic considering the glycans of different types, quantities,

sizes, charges, and rigidity, the biosynthesis is finely controlled by many different enzymes. However, these enzymes usually have more than one target molecule, and the monosaccharides available for glycan synthesis are affected by the cell's metabolism. Thus, different metabolic states (e.g., cancer) alter the biophysical properties of the glycocalyx[7,10].

Interestingly, it recently became evident that the glycocalyx can physically influence receptor organization[15,16] and control the diffusion of receptors via molecular crowding[17] on the cell surface. In addition to the consensus on the heterogeneous mobility and constraints on membrane protein lateral diffusion due to membrane rafts, protein-lipid interactions, and cytoskeletal interactions[18–20], glycocalyx components also have a vital role in limiting protein mobility (i.e., the pericellular coat formed by HA bound to CD44)[21]. These examples show the importance of the glycocalyx in regulating membrane protein dynamics. However, biophysical frameworks to understand and predict the role of these interactions remain limited. The main reason for this limitation is the complexity of the PM and the glycocalyx components, and the very fast (milliseconds) temporal and small (nanometers) spatial scales of above-mentioned interactions. Thus, it is essential to elucidate the biophysical determinants (e.g., size, charge, and structure) of the glycocalyx-protein interactions by tuning the glycocalyx composition and biophysical properties in well-defined synthetic model systems.

Model membranes are widely used to mimic the PM and balance controllable complexity and specificity with the highest physiological relevance[22]. One such example are Giant unilamellar vesicles (GUVs), cell sized free standing lipid vesicles. GUVs can be reconstituted with cell surface proteins. Moreover, fluorescence probes attached to the proteins can be used for dynamics studies via fluorescence correlation spectroscopy (FCS). FCS is a technique to measure the diffusion coefficients of proteins from obtained intensity fluctuations in the focal volume. We recently published a robust method to prepare proteinated GUVs and measure their mobility[23]. GUVs are composed of phospholipids and nickelated lipids that can be functionalized with Histidine (His)-tagged proteins via nickel/His-tag binding. This approach is useful as synthetic biology toolbox for elucidating the effect of glycans on surface proteins.

Here, we first used the reconstitution approach to functionalize GUVs with highly glycosylated receptors in the absence of intracellular and transmembrane domains but present extracellular domain (ECD), where the glycosylation takes place. We found that glycoprotein diffusion decreases as the absolute molecular weight increases but is not correlated with the predicted amino acids weight (PMW_{aa}) based on the amino acid sequences. We then mimicked the glycocalyx-protein interactions by functionalizing GUVs with CD44 attached to HA of different sizes. We found that CD44 diffusion decreases with increasing HA sizes. Finally, we checked the impact of HA on sphingomyelin (SM) dynamics in the presence and absence of CD44. We observed that although HA decreases the diffusion of SM but not DPPE, as CD44 was introduced, SM diffusion was not affected by HA anymore except for the ultra-small HA. Our data suggest a crucial role of the glycocalyx components on MP dynamics in health and disease, and the synthetic toolbox used here can be extended for other interesting questions in the field.

MATERIALS AND METHODS

Lipids, proteins, carbohydrates, and fluorescent dyes

1-palmitoyl-2-oleoyl-sn-glycero-3-phosphocholine (POPC) and 1,2-dioleoyl-sn-glycero-3-[(N-(5-amino-1-carboxypentyl)iminodiacetic acid)succinyl] (nickel salt) (18:1 DGS-NTA(Ni)) (shortly called DOGS NTA) were purchased from Avanti Polar Lipids. All lipid stock solutions (in chloroform) were stored under a stream of nitrogen in a glass at -20 °C.

His-tagged recombinant proteins of cluster of differentiation (CD) 44 (Cat.# 12211-H08H; UniProtKB-P16070, Met 1-Pro 220; molecular weight (MW): 43 kDA, PMW_{aa}: 23.4 kDA), CD34 (Cat.# 10103-H08H; NCBI-NP_001020280.1, Met 1-Thr 290; MW: 40 kDA, PMW_{aa}: 29 kDA), and Integrin alpha 5 beta 1 (Integrin) (Cat.# CT014-H2508H; ITGA5, UniProtKB-P08648, Met 1-Tyr 995; ITGB1, UniProtKB-P05556-1, Met 1-Asp 728; MW: 260 kDA, PMW_{aa}: 192 kDA) were obtained from SinoBiological, and Podocalyxin (PODXL) (Cat.# 1658-PD; NCBI-AAB61574.1, Ser 23-Arg 427; MW: 165 kDA, PMW_{aa}: 43 kDA) and PODXL2 (Cat.# 1524-EG; UniProtKB-Q9NZ53, Gly 33-Thr 500; MW: 110 kDA, PMW_{aa}: 52 kDA) were obtained from R&D Systems.

Given MWs are based on SDS-PAGE under reducing conditions, and their PMW_{aa} are from amino acids sequences.

The different sizes of Hyaluronic acid (HA) were obtained from R&D System: ultra-low MW (Cat.# GLR003, 4.6 kDA), low MW (Cat.# GLR001, 37 kDa), medium MW (Cat.# GLR004, 229 kDa), and high MW (Cat.# GLR002, 1510 kDa).

Note that purchased CD44 from SinoBiological includes four HA binding domain (HABD) (Arg41, Arg78, Tyr79, and Tyr105), important for its conformational switching to bind HA[24].

Abberior STAR Red-1,2-Dipalmitoyl-sn-glycero-3-phosphatidylethanolamine (AbStR-DPPE) and -sphingomyelin (AbStR-SM) were purchased from Abberior GmbH to label the membrane. Alexa Fluor 488 NHS Ester (A488) was obtained from Thermo Fisher for protein labeling.

Protein labeling

The proteins were dissolved in phosphate-buffered saline (PBS) to a concentration of 1 mg/mL and 100 Mm $NaHCO_3$ solution in water (pH 8.5) was added for each 50 µL protein solution. The volume of A488 dye solution which was dissolved in DMSO was calculated based on the formula:

$$V_d = \frac{C_p x V_p}{MW_p} \; x \; ME \; x \; \frac{MW_d}{C_d};$$

C_p–protein concentration (fixed to 1 mg/mL), V_p–volume of protein to label (fixed to 50 µL), MW_p–protein molecular weight, ME–molar excess (number of dye molecules per protein molecule, fixed to 8), MW_d–dye (A448) molecular weight (643.4 g/mol), C_d–concentration of dye solution (fixed to 1 mg/mL), and V_d–the volume of the dye solution. After adding the dye solution to protein solution, it was incubated for 1 hour at RT with continuous stirring at 300 rpm. Purification was performed using spin columns (7 kDa exclusion limit, 0.5 mL Zeba spin desalting columns, ThermoFisher Scientific). The final protein concentration (C_p final) was measured by nanodrop (analyzed by NanoDrop 2000) using extinction coefficients of proteins estimated from ProtParam-Expasy based on amino acid sequences **(Supp. Info. 1)**. The degree of labeling was calculated considering the maximal absorbance of dye and its molar extinction for each protein. Details of protein labeling is in **Supp. Table 1**.

Preparation of biomimetic membranes

Electroformation method was used for GUVs production. A lipid mixture of 1 mg/mL POPC with 1% mol of DOGS NTA was dissolved in chloroform. 5 µL of lipid mixture was spread on platinum wires and dried under a stream of nitrogen. It was then placed into 370 µL 300 mM sucrose solution in a custom-build, Teflon-coated electroformation chamber. 10 Hz AC field (2V) was applied for GUVs production (DG822, Rigol) for 1 hour followed with 2 Hz for 30 mins for GUVs release at RT.

GUVs were labeled and incubated for 30 mins by adding AbStR-DPPE or AbStR-SM as a membrane dye and A488-labeled proteins for histidine-nickel coupling to a final concentration of 100 ng/mL and 5-10 µg/mL (around equal moles), respectively. GUVs were washed once with their 3-fold volume of PBS to reduce the background signal by unbound dye. GUVs sink to the bottom of the tube after 30 mins due to the density difference between sucrose and PBS. An initial volume of GUVs can then be taken with cut pipette tips to reduce shear stress and used for measurements. For HA experiments, an extra washing step was performed after 30 mins HA incubation (10 µg/mL, the same for all HA).

Confocal imaging and FCS were performed in Ibidi 8-well glass-bottom chambers (#1.5H). To prevent bursting and immobilize GUVs, the chambers were coated with bovine serum albumin (BSA) (Sigma-Aldrich, 3 mg/mL in PBS) for 1 h and washed 3 times with PBS.

Confocal imaging and FCS measurements

A Zeiss LSM 980 confocal laser scanning microscope equipped with a 40x 1.2 water-immersion objective was used for imaging and FCS experiments. Green and far-red fluorescence were excited with 488 nm and 639 nm lasers and their fluorescent emission collected in two channels within the spectral windows of 499–561 nm and 641–694 nm, respectively. The pinhole parameter was set to 1 Airy Unit. The dynamic range was automated, with four times line averaging. The confocal image was taken by positioning the focal plane at the GUV equatorial plane.

For FCS measurements, the calibration of the pinhole position and the correction collar of the objective for FCS was performed before the measurement using Alexa 488 solution (5 ng/mL) in water in the same Ibidi chamber as the samples. Green and

far-red fluorescence were excited with 488 nm and 639 nm lasers and their fluorescent emission collected in two channels within the spectral windows of 499–597 nm and 641–694 nm, respectively. The pinhole parameter was set to 1 Airy Unit. The focal plane was roughly positioned at the bottom of GUVs, and z-scan was performed in the range of 3 µm with 0.5 µm intervals. The position for the highest intensity overlap between two channels was chosen to obtain 5 seconds FCS curves with 6 repetitions with low laser power. The obtained correlation curves were fit and analyzed by FoCuS-point software[25]. The data was visualized and statistically analyzed by GraphPad Prism 9.

RESULTS AND DISCUSSION

We utilized GUVs as a biomimetic membrane system to establish a platform for investigating the glycocalyx-protein interactions. GUVs have various advantages: most importantly, the parameters of the vesicle content and organization can be controlled, such as the lipid and protein composition, size, and charge properties. In addition, the direct effect of introduced molecules (e.g., proteins or sugars) can be investigated since there are no other complementary pathways that can normally disrupt such observations in native cells. They also enable visualization under the microscope for a long time period and generally do not show phototoxicity and death. Thus, we investigated the impact of the glycocalyx components on MPs diffusion in GUVs.

Protein reconstitution in GUVs

We first generated homogenous GUVs (POPC) with 1 mol% of DOGS NTA to elucidate the role of protein MW shaped by glycosylation, the most common form of posttranslational modification, on glycoproteins diffusion **(Fig. 1A)**. POPC is an monounsaturated lipid and exhibits a high viscosity in model membranes[26], creating a more sensitive model to recognize small differences in diffusion. Nickelated lipids can directly bind to His-tagged proteins, and BSA coated imaging chamber enables the immobilization of GUVs for accurate FCS measurements. To visualize and recognize the GUVs, adjust the focal plane, and have a reference for diffusion coefficient, we labeled vesicles with the membrane dye called AbStR-DPPE. To

visualize the ECDs of glycoproteins (GlyP-ECD) attached to nickelated lipids, we used A488. We observed that GlyP-ECD in GUVs with DOGS NTA partition homogenously in the vesicles, creating a reliable platform for diffusivity measurements **(Fig. 1B)**.

To investigate the diffusion of highly glycosylated GlyP-ECD, we reconstituted the proteins responsible for complex signaling events in the PM, such as cell-cell interactions, cell adhesion, cell migration, cell morphology, and cancer progression: CD44, CD34, PODXL, PODXL2, and integrin. The estimated size of the GlyP-ECD from PDB, their absolute MW from SDS-PAGE under reducing conditions, and their PMW_{aa} from amino acids sequences are shown in **Fig. 1C**. The primary sequences of the GlyP-ECD are shown in **Supp. Info. 1**.

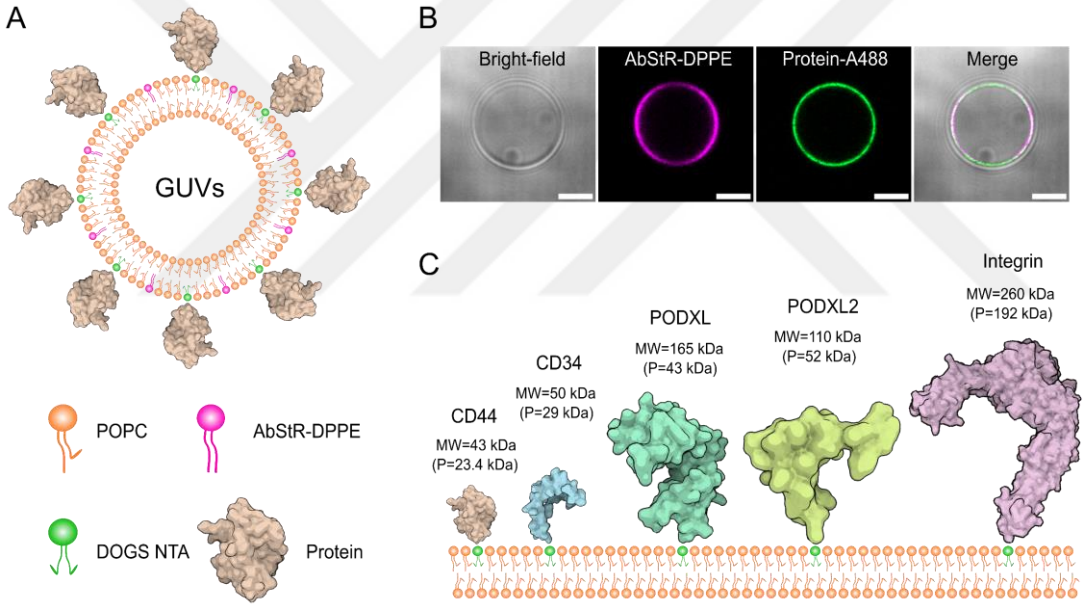

Fig. 1. Protein reconstitution in GUVs via nickel/His-tag binding. A) Cartoon representation of POPC GUVs with DOGS NTA and AbStR-DPPE. B) Bright-field and fluorescent confocal microscopy imaging of GUVs, where the proteins are labeled with A488. Scale bar is 5 µm. C) GlyP-ECD reconstitution in GUVs and their predicted weights and absolute MWs information. The sizes of the proteins are representative based on MWs.

Glycoproteins diffusion is shaped by the attachment of glycans

Lateral diffusion of MPs is an essential physical parameter to acquire a mechanistic understanding of both proteins and membrane dynamics[27]. Saffman and Delbrück's

model on protein diffusion suggests a weak logarithmic reciprocal correlation between the radius of the protein and its diffusion with the assumptions of unlimited lipid bilayers and surrounding liquids, and the cylindrical shape of embedded proteins[28]. There have been some corrections[5,29–34] and also disagreements[35] to this model with revised assumptions and better experimental approaches. The main controversy was raised for several reasons: (1) some experiments did not consider lipids diffusion together with the proteins to have a control system to ensure the only variable is the protein, or when the data used in theoretical work was taken from different papers, these different data were not normalized by the lipids diffusion; (2) variations between different methods (e.g., FCS and fluorescence recovery after photobleaching) used for diffusion measurements were not well considered[36]; (3) protein reconstitution methods and model membrane systems varied too much that some drawbacks (e.g., surface hindrance in support lipid bilayers) were not paid attention[37]. However, the most important reason lacking in the literature is that the production host (e.g., eukaryotes vs. prokaryotes, or the same protein from different eukaryotic hosts) and conditions (e.g., extraction protocols and upstream process) of these proteins, which determine the abundance and specific biophysics of glycans attached to the proteins (e.g., size, species, charge, flexibility, and shape)[38,39], may affect the overall folding thus structure and radius of the protein. Moreover, X-ray crystallography studies are generally difficult on glycoproteins and require deglycosylation to some extent which could lead to misinterpretation of defined protein radius used in theoretical frameworks for the diffusion studies[40].

Mentioned papers about lateral diffusion of MPs mainly consider proteins totally embedded in the lipid bilayers thereby ignoring the effect of ECD. It has been recently shown that the diffusion of MPs is also influenced by the ECDs[23,41–44], domain susceptible to glycans. N or O-glycosylation can regulate the biophysics of the MPs and possibly alter their function, offering a different, complementary, and additional information content besides the protein sequences[45,46]. Thus, the glycomics of the ECDs plays a significant role in MP dynamics. To elucidate the bulk effect of glycans on glycoprotein diffusion, we employed FCS to measure the diffusion coefficient of highly glycosylated GlyP-ECD **(Fig. 2A)** and then compared them with two other surface proteins (ICAM-1 and CD45) from the literature which have a similar PMW_{aa} with one of the GlyP-ECD used in the experiment. We

observed some cluster formations of integrin in the confocal image while performing FCS measurements due possibly to the labeling issue of a big protein, resulting in a different fitting pattern in the autocorrelation curve. We first investigated how the mobility of the GlyP-ECD was affected by their absolute MWs in GUVs. We observed that GlyP-ECD diffusion decreases with increasing absolute MWs **(Fig. 2B)**. In the same experimental conditions, there was no change in membrane dye diffusion in GUVs with GlyP-ECD of different weights, suggesting that other parameters (e.g., the thickness of the imaging chamber, adjustment of the focal plane for FCS measurement, temperature, and membrane fluidity) did not affect the observed difference in the diffusion for different GlyP-ECD **(Fig. 2C)**. Since molecular crowding is a crucial parameter of the diffusivity of molecules, we also compared the number of molecules with the diffusion coefficients for each GlyP-ECD. There is no particular inverse linear relationship between the number of molecules in the focal plane and the diffusion coefficient for any of GlyP-ECD, suggesting that observed results were not caused by molecular crowding but indeed due to the MW of GlyP-ECD **(Supp. Info. 2)**. All the following experiments were also performed in similar concentrations thus in the same dilute conditions.

One striking observation about the effect of glycans on GlyP-ECD dynamics was that the diffusion of PODXL was slower than PODXL2. As indicated by the commercial provider, although PODXL (P=43 kDa) is lighter than PODXL2 (P=52 kDa) in PMW_{aa}, PODXL (MW=165 kDa) was heavily glycosylated and thus heavier than PODXL2 (MW=110 kDa) in absolute MW, which was reflected in the diffusion by PODXL2 being significantly faster than PODXL **(Fig. 2B)**. We then used diffusion coefficients of ICAM-1 (lightly glycosylated) and CD45 (heavily glycosylated) from the literature and compared them with our GlyP-ECD after normalizing them by lipid diffusion[23]. ICAM-1 (P=51 kDa) has a very similar PMW_{aa} compared to PODXL2 but is relatively less glycosylated (MW=70 kDa). Despite having similar PMW_{aa}, PODXL2 was significantly slower than ICAM-1, further justifying the mobility hindrance effect of glycans attachment to GlyP-ECD. Likewise, although CD45 (P=57.4 kDa, MW=116) is heavier than both PODXL and PODXL2 in PMW_{aa}, it has a similar absolute MW with PODXL2 and lower MW than PODXL, further confirming our hypothesis by observing non-significant difference between CD45 and PODXL2 but CD45 being significantly faster than PODXL.

We concluded that the diffusion of GlyP-ECD decreases as the absolute MW of the GlyP-ECD increases due to glycosylation but is not correlated with PMW_{aa} based on their amino acid sequences. Although the bulk effect of glycans on GlyP-ECD diffusion is clear, the conclusion from the diffusion study should be interpreted with caution for a reason: performed experimental method is limited to the bulk effect of glycans on GlyP-ECD diffusion but not individual biophysical effects of glycans (e.g., species, structure, charge, or size).

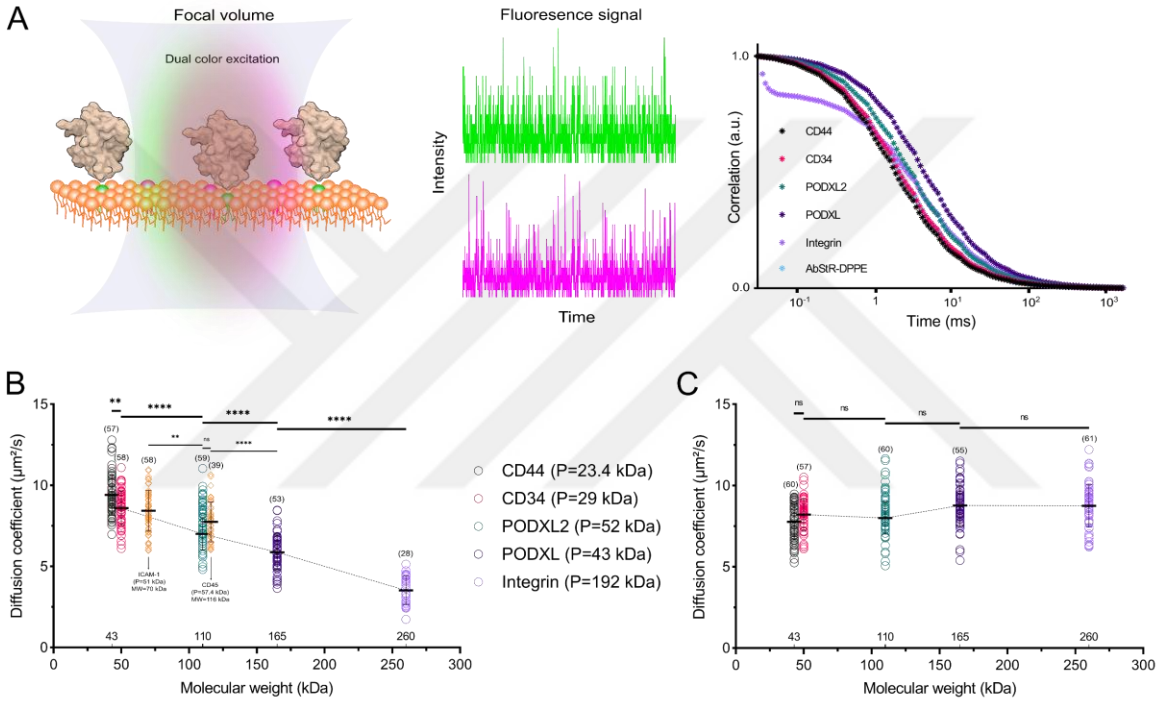

Fig. 2. Glycans are critical for glycoproteins diffusion in GUVs. A) Cartoon representation of FCS experiment, where the protein of interest and membrane lipids attached to fluorescence dyes are excited with two lasers, their fluorescent intensity fluctuations are captured, and autocorrelation curves are fitted for all GlyP-ECD individually together with membrane dye. B) Diffusion coefficient of GlyP-ECDs and C) membrane dye in POPC GUVs. While absolute MWs of GlyP-ECDs are indicated in x-axes, their PMW_{aa} is shown as P in the legends. The means of each GlyP-ECD are connected with lines. Student's t-test (two-tailed, non-parameterized) was used to determine significance (****P<0.0001; CD44/CD34: P=0.0017; ns stands for non-significant: P>0.05). Diffusion data of two additional proteins were taken from Wedemann et al. after normalization[23] (ICAM-1/PODXL2: P=0.0021). Error bars represent the standard deviation. The numbers of data points obtained from experiments are indicated on the graphs in parentheses.

HA size determines CD44 diffusion

To address the above-mentioned caution and create a more controlled system for the binding of glycans to GlyP-ECD, we first reconstituted CD44 in GUVs as previously described and then introduced HA of different sizes to form CD44-HA complexes **(Fig. 3A)**. The established model was independent from the stochastic effect of glycosylation on different proteins since the same protein, CD44, was reconstituted. The model was based on the same glycan, HA, composing of repeating disaccharide units, thus other biophysical parameters were the same but the size. To test the effect of HA size on the protein diffusion, we next performed FCS measurements on GUVs reconstituted with CD44. FCS measurements were conducted with non-labeled HA to eliminate the possible cross-linking artifacts. Instead, CD44 and membrane were labeled with A488 and AbStR-DPPE, respectively. We used four different sizes of HA, ranging from 4.6 to 1510 kDa, and observed a clear decrease in diffusion of CD44 as the HA size increased **(Fig. 3B)**. In the same experimental setup, there was no change in membrane dye diffusion in GUVs with CD44-HA complexes, suggesting that other parameters did not affect the observed difference in the diffusion of CD44 treated with HA of different sizes **(Fig. 3C)**. It further confirmed the hindrance effect of glycans on protein diffusion. In addition, to test if the observed effect was specific to CD44-HA interaction via HABD, we performed the same experiment by reconstituting PODXL in GUVs, as previously described. We observed no difference in diffusion with and without HA treatment for PODXL, indicating that HA binding and related decrease in diffusion is specific to CD44 but not to other proteins **(Fig. 3B)**.

By investigating the glycans effect on protein diffusion with CD44-HA complex, we created a relatively more controlled system and addressed the causations mentioned before. Although our results suggest a decreasing trend as HA size increases, the data points for the first groups were rather dispersed, reflecting the limitations of the system. First, the number of HA bound to each CD44 within the same HA group is unpredictable. While HABDs of some CD44 in GUVs are more accessible, it may not be for other CD44 due to their diverse orientation in the membrane. It is probably not a big concern considering the same environment (e.g., pH, salt, temperature) of CD44-HA complexes in the same HA group. Second, the binding affinity of each HA is different and related to their sizes. The maximum binding occurs around 1000

kDa[47], meaning that considering the amount of HABDs, the average number of HA and their stability per CD44 for the largest HA could be bigger than the smallest HA, leading to a narrower binding distribution of bigger HAs. This could be the reason for dispersed data seen only for the smallest HAs **(Fig. 3B)**. It is not a disadvantage but rather a richness of the system by showing the binding affinity difference from a different perspective. Third, the most important concern and also the reason behind the reproducibility problem of the system is that CD44 in some cells does not constitutively bind HA[48], which means that it is not certain that all CD44 proteins in our system were active state and bound to HA. This could create a heterogeneity of active and inactive states of CD44 in our system and could explain the dispersity of the data and the problem of reproducibility. However, there have been suggested solutions to this problem, such as treatment of CD44 with specific monoclonal antibodies or inducers (e.g., phorbol ester) that can increase the binding affinity of HA[49]. Such treatments of proteins before the measurements could be useful for a more reliable experimental setup.

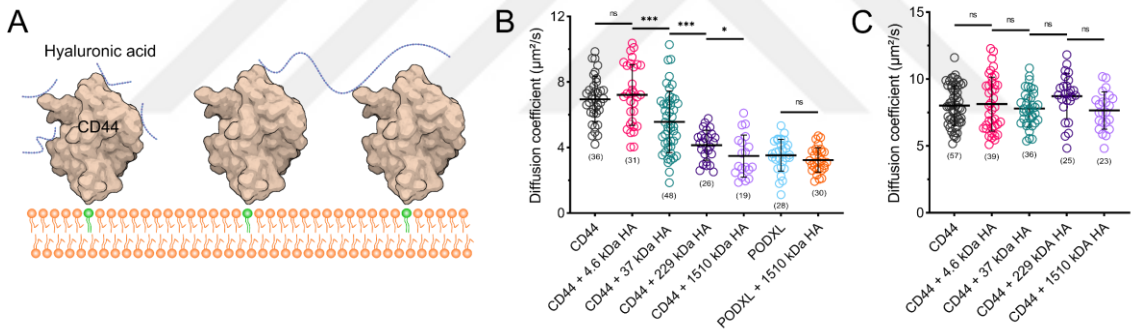

Fig. 3. HA size determines CD44 diffusion in GUVs. A) Cartoon representation of binding of CD44 to HA of different sizes. B) Diffusion coefficient of CD44 and PODXL and C) membrane dye with and without HA treatment in POPC GUVs. Student's t-test (two-tailed, non-parameterized) was used to determine significance (CD44 + 4.6 kDa HA/CD44 + 37 kDa: P=0.0003; CD44 + 37 kDa HA/CD44 + 229 kDa: P=0.0007; CD44 + 229 kDa HA/CD44 + 1510 kDa: P=0.0435; ns stands for non-significant: P>0.05). Error bars represent the standard deviation. The numbers of data points obtained from experiments are indicated on the graphs in parentheses.

CD44 competes with SM for HA binding

In addition to our motivation of establishing a more controlled system to investigate the impact of binding of glycans to GlyP-ECD, CD44-HA complex is an important lipid-protein-carbohydrate interplay for biology. CD44 is a multifunctional protein,

highly expressed in cancer cells and responsible for regulating metastasis[50]. Its ligand, HA, has size-specific biological activities. While low molecular weight (LMW) HA is pro-inflammatory, high molecular weight (HMW) HA is anti-inflammatory[51–54]. This dual nature of CD44-HA complex suggests that CD44-HA both promotes and inhibits cancer progression[55]. It recently became evident that sphingolipid metabolites are also responsible for regulating inflammation[56–58]. In addition, it is shown that glycans (including HA) have a profound effect on the nanoscale lipid organization of the membranes enriched in sphingolipids[59,60]. These seemingly unrelated biomolecules (CD44, HA, and sphingolipids) are somehow interacting and involved in inflammation. As HA interacts with sphingolipids and changes their dynamics, to determine the role of CD44 in this interaction, we used our reconstitution strategy to investigate the competition between CD44 and sphingolipids for HA **(Fig. 4A)**.

To test the effect of HA on SM diffusion, we first performed FCS measurements on GUVs labeled with AbStR-SM or AbStR-DPPE. While there was no change in diffusion of AbStR-DPPE in the presence of HA, there was a clear decrease in the diffusion coefficient of AbStR-SM treated with HA, confirming that HA interacts with SM but not with DPPE and slows down the diffusion of SM **(Fig. 4B)**. This possible interaction between SM and HA due to their high hydrogen-bonding capacity (via OH groups of HA and the NH groups of SM) was suggested in the literature[61–63]. To elucidate the role of CD44 in HA-SM interaction, we next performed FCS measurements on GUVs reconstituted with CD44 and labeled with AbStR-SM. There was no difference in the diffusion of SM between the GUVs non-treated and treated with HA of different sizes except the ultra-small HA (4.6 kDA), suggesting that CD44 has early access to HA and blocks the possible interaction spaces for HA-SM binding **(Fig. 4C)**. However, ultra-small HA can probably penetrate through the gaps between different CD44 proteins and still interact with SM and thus change SM diffusion.

Interestingly, it is recently suggested that during the infection of macrophages by *Staphylococcus aureus,* hydrolysis of sphingomyelins results in ceramide formations and CD44 can cluster in ceramide-enriched membrane domains and prevents the sepsis, a consequence of inflammation[64]. Although the proposed model considers the actin cytoskeleton and CD44 interplay, possible interaction dynamics at the cell surface by HA are neglected. Our results could be complementary to the proposed model that overproduction and clustering of CD44 may facilitate the binding of HA to

CD44 and prevent LMW HAs from binding to SM, which is normally pro-inflammatory. In our model, without CD44 clustering, CD44 heavily competed with SM for HA binding in the range of LMW. However, the abundance of CD44 in our system was not enough to block the binding of ultra-small HA. In a system, where a higher molar concentration of anchor lipids is used for CD44 attachment, it is possible that CD44 proteins cover the surface enough that it may even block the binding of smaller HAs to SM. In addition, it is indicated in the same paper that filopodia, finger-like protrusions, was significantly less developed in sphingomyelinase deficient macrophages but more prominent in wild-type. This was hypothesized only with actin cytoskeleton dynamics via ezrin and the cytosolic tail of CD44. However, high HA synthesis activity[65] and thus accumulated force by HA[66] at the cell surface has an effect on the density and length of filopodia. Thus, excess CD44-HA complexes due to CD44 clustering by ceramide could be an important regulator for filopodia formation.

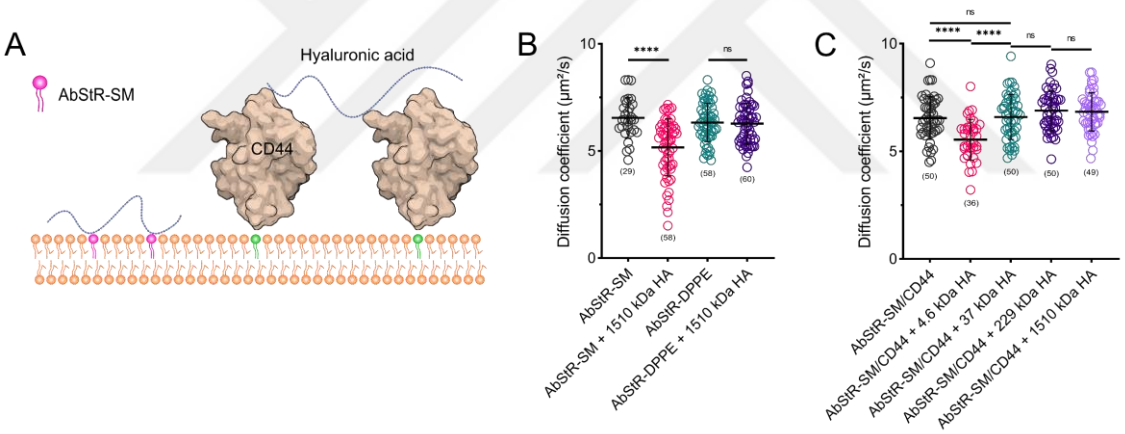

Fig. 4. HA determines the SM diffusion only in the absence of CD44 except for the ultra-small HA. A) Cartoon representation of HA bound to SM labeled with AbStR and to CD44. B) Diffusion coefficient of AbStR-SM and AbStR-DPPE in the presence and absence of HA in GUVs. C) Diffusion coefficient of AbStR-SM after addition of HAs of different sizes in GUVs with CD44. Student's t-test (two-tailed, non-parameterized) was used to determine significance (****P<0.0001; ns stands for non-significant: P>0.05). Error bars represent the standard deviation. The numbers of data points obtained from experiments are indicated on the graphs in parentheses.

CONCLUSION AND LIMITATIONS

Constraints in MP diffusion are largely attributed to the actin cytoskeleton, membrane rafts, specific lipid-protein interactions, and molecular crowding. Often overlooked is that the glycocalyx also can create constraints on MP diffusion. In this project, we examined the role of the glycocalyx on MP dynamics. Our data show both bulk and size-dependent hindrance effect of glycans on MP diffusion. In addition, our results show the competition between CD44 and SM for HA binding, which could be a regulation system for inflammation. It is also important to mention the limitation of the study. Absence of molecular crowding (i.e., other membrane lipids and proteins), reconstitution of only ECD (i.e., absence of full-length protein), and absence of intracellular and other extracellular components (i.e., actin cytoskeleton and extracellular matrix) could be other contributors to observed results. Therefore, the knowledge transition from GUVs to native PM requires caution. Despite of mentioned limitations, our system enables a robust, controllable, and easy platform to elucidate the role of the glycocalyx on the membrane and MP dynamics. These studies are essential since the elucidation of carbohydrates-lipids-proteins interplay can lead to potential therapies for various diseases.

FUTURE WORK

Non-accurate reflection of physiological conditions is the main disadvantage of synthetic model membranes. Native plasma membrane components (i.e., lateral heterogeneity) may be needed for controlling the processes of the glycocalyx-protein interactions. Giant plasma membrane vesicles[22] (GPMVs) that reflect the lateral heterogeneity to a large extent can be employed to establish an intermediate system. Drug-treated cell-derived membranes with modified glycocalyx can be used to elucidate the glycocalyx-protein interactions isolated from the effect of the cytoskeleton and also in high protein and lipid diversity. Therefore, GPMVs could be a crucial semi-native platform to test mentioned interactions. In addition, the top-down approach should be performed as a comparative and complementary method. Valuable findings taken from model systems enable to focus on certain parameters and manipulate them in top-down experiments. Hence, combining two methods is required to achieve conclusive findings about the biophysical principles of the

glycocalyx-proteins interactions. For example, we could use several different congenital disorders of glycosylation cell models, which show a deficiency in the glycocalyx. In addition, we could employ genome engineering methods such as CRISPR/Cas9 to alter the glycoprotein expression level or content. Moreover, we may use different drugs or enzymes to disrupt the glycocalyx. All will create cells lacking certain glycocalyx components with mentioned ways, and we can quantify their effects on protein dynamics.

ETHICAL REFLECTION

All the experiments were performed on non-living systems. When results from this project are published, the raw data will be available for others. Considering the sustainable development goals of good health and well-being and responsible consumption and production, the results from this study could contribute to a better understanding of health, and extra attention was given to the adequate consumption of some reagents and lab equipment used in the study.

ACKNOWLEDGEMENTS

I would like first to thank my supervisors, Taras Sych and Erdinc Sezgin, and all CSI:Nano lab members (https://www.csi-nano.org/members.html) for teaching me how to think scientifically and become an effective skeptic when the time comes. I also thank Dirk Ollech for his constructive feedback on the thesis and SciLifeLab Advanced Light Microscopy facility and National Microscopy Infrastructure (VR-RFI 2016-00968) for microscopy imaging. The figures were prepared by Inkscape and BioRender.

REFERENCES

1. Singer, S. J. & Nicolson, G. L. The Fluid Mosaic Model of the Structure of Cell Membranes. *Science* **175**, 720–731 (1972).
2. Simons, K. & Ikonen, E. Functional rafts in cell membranes. **387**, 4 (1997).
3. Kusumi, A. & Sako, Y. Cell surface organization by the membrane skeleton. *Current Opinion in Cell Biology* **8**, 566–574 (1996).
4. Kwik, J. *et al.* Membrane cholesterol, lateral mobility, and the phosphatidylinositol 4,5-bisphosphate-dependent organization of cell actin. *Proc. Natl. Acad. Sci. U.S.A.* **100**, 13964–13969 (2003).
5. Goose, J. E. & Sansom, M. S. P. Reduced Lateral Mobility of Lipids and Proteins in Crowded Membranes. *PLOS Computational Biology* **9**, e1003033 (2013).
6. Schneider, F. *et al.* Diffusion of lipids and GPI-anchored proteins in actin-free plasma membrane vesicles measured by STED-FCS. *Mol Biol Cell* **28**, 1507–1518 (2017).
7. Kuo, J. C.-H., Gandhi, J. G., Zia, R. N. & Paszek, M. J. Physical biology of the cancer cell glycocalyx. *Nature Phys* **14**, 658–669 (2018).
8. Wardzala, C. L., Wood, A. M., Belnap, D. M. & Kramer, J. R. Mucins Inhibit Coronavirus Infection in a Glycan-Dependent Manner. *ACS Cent. Sci.* **8**, 351–360 (2022).
9. Kanyo, N. *et al.* Glycocalyx regulates the strength and kinetics of cancer cell adhesion revealed by biophysical models based on high resolution label-free optical data. *Sci Rep* **10**, 22422 (2020).
10. Gandhi, J. G., Koch, D. L. & Paszek, M. J. Equilibrium Modeling of the Mechanics and Structure of the Cancer Glycocalyx. *Biophysical Journal* **116**, 694–708 (2019).
11. Shurer, C. R. *et al.* Physical Principles of Membrane Shape Regulation by the Glycocalyx. *Cell* **177**, 1757-1770.e21 (2019).
12. Bertozzi, C. R. & Kiessling, L. L. Chemical Glycobiology. **291**, 9 (2001).

13. Möckl, L. The Emerging Role of the Mammalian Glycocalyx in Functional Membrane Organization and Immune System Regulation. *Front. Cell Dev. Biol.* **8**, 253 (2020).
14. Krasnova, L. & Wong, C.-H. Understanding the Chemistry and Biology of Glycosylation with Glycan Synthesis. *Annu. Rev. Biochem.* **85**, 599–630 (2016).
15. Paszek, M. J. *et al.* The cancer glycocalyx mechanically primes integrin-mediated growth and survival. *Nature* **511**, 319–325 (2014).
16. Liu, P. *et al.* The Formation and Stability of DC-SIGN Microdomains Require its Extracellular Moiety: DC-SIGN Microdomains Require Extracellular Moiety. *Traffic* **13**, 715–726 (2012).
17. Chapanian, R. *et al.* Enhancement of biological reactions on cell surfaces via macromolecular crowding. *Nat Commun* **5**, 4683 (2014).
18. Kusumi, A. *et al.* Dynamic Organizing Principles of the Plasma Membrane that Regulate Signal Transduction: Commemorating the Fortieth Anniversary of Singer and Nicolson's Fluid-Mosaic Model. *Annu. Rev. Cell Dev. Biol.* **28**, 215–250 (2012).
19. Sezgin, E., Levental, I., Mayor, S. & Eggeling, C. The mystery of membrane organization: composition, regulation and roles of lipid rafts. *Nat Rev Mol Cell Biol* **18**, 361–374 (2017).
20. Fujiwara, T. K. *et al.* Confined diffusion of transmembrane proteins and lipids induced by the same actin meshwork lining the plasma membrane. *MBoC* **27**, 1101–1119 (2016).
21. Freeman, S. A. *et al.* Transmembrane Pickets Connect Cyto- and Pericellular Skeletons Forming Barriers to Receptor Engagement. *Cell* **172**, 305-317.e10 (2018).
22. Sych, T., Gurdap, C. O., Wedemann, L. & Sezgin, E. How Does Liquid-Liquid Phase Separation in Model Membranes Reflect Cell Membrane Heterogeneity? *Membranes* **11**, 323 (2021).

23. Wedemann, L., Gurdap, C. O., Sych, T. & Sezgin, E. The influence of the extracellular domains on the dynamic behavior of membrane proteins. *bioRxiv* 2021.11.15.468619 (2021) doi:10.1101/2021.11.15.468619.
24. Jamison, F. W., Foster, T. J., Barker, J. A., Hills, R. D. & Guvench, O. Mechanism of binding site conformational switching in the CD44-hyaluronan protein-carbohydrate binding interaction. *J Mol Biol* **406**, 631–647 (2011).
25. Waithe, D., Clausen, M. P., Sezgin, E. & Eggeling, C. FoCuS-point: software for STED fluorescence correlation and time-gated single photon counting. *Bioinformatics* **32**, 958–960 (2016).
26. Beckers, D., Urbancic, D. & Sezgin, E. Impact of Nanoscale Hindrances on the Relationship between Lipid Packing and Diffusion in Model Membranes. *J. Phys. Chem. B* **124**, 1487–1494 (2020).
27. Jacobson, K., Liu, P. & Lagerholm, B. C. The Lateral Organization and Mobility of Plasma Membrane Components. *Cell* **177**, 806–819 (2019).
28. Saffman, P. G. & Delbrück, M. Brownian motion in biological membranes. *PNAS* **72**, 3111–3113 (1975).
29. Frick, M., Schmidt, K. & Nichols, B. J. Modulation of Lateral Diffusion in the Plasma Membrane by Protein Density. *Current Biology* **17**, 462–467 (2007).
30. Petrov, E. P. & Schwille, P. Translational Diffusion in Lipid Membranes beyond the Saffman-Delbrück Approximation. *Biophysical Journal* **94**, L41–L43 (2008).
31. Ramadurai, S. *et al.* Lateral Diffusion of Membrane Proteins. *J. Am. Chem. Soc.* **131**, 12650–12656 (2009).
32. Morozova, D., Guigas, G. & Weiss, M. Dynamic Structure Formation of Peripheral Membrane Proteins. *PLOS Computational Biology* **7**, e1002067 (2011).

33. Weiß, K. *et al.* Quantifying the Diffusion of Membrane Proteins and Peptides in Black Lipid Membranes with 2-Focus Fluorescence Correlation Spectroscopy. *Biophys J* **105**, 455–462 (2013).
34. Guigas, G. & Weiss, M. Size-Dependent Diffusion of Membrane Inclusions. *Biophys J* **91**, 2393–2398 (2006).
35. Gambin, Y. *et al.* Lateral mobility of proteins in liquid membranes revisited. *Proceedings of the National Academy of Sciences* **103**, 2098–2102 (2006).
36. Calizo, R. C. & Scarlata, S. Discrepancy between fluorescence correlation spectroscopy and fluorescence recovery after photobleaching diffusion measurements of G-protein-coupled receptors. *Anal Biochem* **440**, 40–48 (2013).
37. Castellana, E. T. & Cremer, P. S. Solid supported lipid bilayers: From biophysical studies to sensor design. *Surf Sci Rep* **61**, 429–444 (2006).
38. Gupta, S. K. & Shukla, P. Glycosylation control technologies for recombinant therapeutic proteins. *Appl Microbiol Biotechnol* **102**, 10457–10468 (2018).
39. Butler, M. & Spearman, M. The choice of mammalian cell host and possibilities for glycosylation engineering. *Current Opinion in Biotechnology* **30**, 107–112 (2014).
40. Davis, S. J. *et al.* Expression of soluble recombinant glycoproteins with predefined glycosylation: application to the crystallization of the T-cell glycoprotein CD2. *Protein Eng Des Sel* **6**, 229–232 (1993).
41. Wieser, S., Moertelmaier, M., Fuertbauer, E., Stockinger, H. & Schütz, G. J. (Un)Confined Diffusion of CD59 in the Plasma Membrane Determined by High-Resolution Single Molecule Microscopy. *Biophysical Journal* **92**, 3719–3728 (2007).
42. Hartel, A. J. W. *et al.* The molecular size of the extra-membrane domain influences the diffusion of the GPI-anchored VSG on the trypanosome plasma membrane. *Sci Rep* **5**, 10394 (2015).

43. Houser, J. R. *et al.* The impact of physiological crowding on the diffusivity of membrane bound proteins. *Soft Matter* **12**, 2127–2134 (2016).
44. Kim, D.-H. *et al.* Analysis of Interactions between the Epidermal Growth Factor Receptor and Soluble Ligands on the Basis of Single-Molecule Diffusivity in the Membrane of Living Cells. *Angewandte Chemie* **127**, 7134–7138 (2015).
45. Mitra, N., Sinha, S., Ramya, T. N. C. & Surolia, A. N-linked oligosaccharides as outfitters for glycoprotein folding, form and function. *Trends in Biochemical Sciences* **31**, 156–163 (2006).
46. Walsh, C. T., Garneau-Tsodikova, S. & Gatto, G. J. Protein Posttranslational Modifications: The Chemistry of Proteome Diversifications. *Angew. Chem. Int. Ed.* **44**, 7342–7372 (2005).
47. Jiang, L. *et al.* Molecular weight impact on the mechanical forces between hyaluronan and its receptor. *Carbohydrate Polymers* **197**, 326–336 (2018).
48. Lesley, J., Kincade, P. W. & Hyman, R. Antibody-induced activation of the hyaluronan receptor function of CD44 requires multivalent binding by antibody. *Eur J Immunol* **23**, 1902–1909 (1993).
49. Lesley, J., Hascall, V. C., Tammi, M. & Hyman, R. Hyaluronan Binding by Cell Surface CD44*. *Journal of Biological Chemistry* **275**, 26967–26975 (2000).
50. Senbanjo, L. T. & Chellaiah, M. A. CD44: A Multifunctional Cell Surface Adhesion Receptor Is a Regulator of Progression and Metastasis of Cancer Cells. *Frontiers in Cell and Developmental Biology* **5**, (2017).
51. West, D. C., Hampson, I. N., Arnold, F. & Kumar, S. Angiogenesis Induced by Degradation Products of Hyaluronic Acid. *Science* **228**, 1324–1326 (1985).
52. Stern, R. Hyaluronan catabolism: a new metabolic pathway. *Eur J Cell Biol* **83**, 317–325 (2004).

53. Itano, N. & Kimata, K. Mammalian hyaluronan synthases. *IUBMB Life* **54**, 195–199 (2002).
54. Deed, R. *et al.* Early-response gene signalling is induced by angiogenic oligosaccharides of hyaluronan in endothelial cells. Inhibition by non-angiogenic, high-molecular-weight hyaluronan. *International Journal of Cancer* **71**, 251–256 (1997).
55. Louderbough, J. M. V. & Schroeder, J. A. Understanding the Dual Nature of CD44 in Breast Cancer Progression. *Molecular Cancer Research* **9**, 1573–1586 (2011).
56. Nixon, G. F. Sphingolipids in inflammation: pathological implications and potential therapeutic targets. *Br J Pharmacol* **158**, 982–993 (2009).
57. Maceyka, M. & Spiegel, S. Sphingolipid metabolites in inflammatory disease. *Nature* **510**, 58–67 (2014).
58. Gault, C., Obeid, L. & Hannun, Y. An overview of sphingolipid metabolism: from synthesis to breakdown. *Adv Exp Med Biol* **688**, 1–23 (2010).
59. Subramaniam, A. B., Guidotti, G., Manoharan, V. N. & Stone, H. A. Glycans pattern the phase behaviour of lipid membranes. *Nature Mater* **12**, 128–133 (2013).
60. Winkler, P. M., Campelo, F., Giannotti, M. I. & Garcia-Parajo, M. F. Impact of Glycans on Lipid Membrane Dynamics at the Nanoscale Unveiled by Planar Plasmonic Nanogap Antennas and Atomic Force Spectroscopy. *J. Phys. Chem. Lett.* **12**, 1175–1181 (2021).
61. Ramstedt, B. & Slotte, J. P. Sphingolipids and the formation of sterol-enriched ordered membrane domains. *Biochimica et Biophysica Acta (BBA) - Biomembranes* **1758**, 1945–1956 (2006).
62. Giannotti, M. I., Rinaudo, M. & Vancso, G. J. Force Spectroscopy of Hyaluronan by Atomic Force Microscopy: From Hydrogen-Bonded Networks toward Single-Chain Behavior. *Biomacromolecules* **8**, 2648–2652 (2007).

63. Mombelli, E., Morris, R., Taylor, W. & Fraternali, F. Hydrogen-Bonding Propensities of Sphingomyelin in Solution and in a Bilayer Assembly: A Molecular Dynamics Study. *Biophysical Journal* **84**, 1507–1517 (2003).
64. LiCao *et al.* Regulation of Staphylococcus aureus Infection of Macrophages by CD44, Reactive Oxygen Species, and Acid Sphingomyelinase. *Antioxidants & Redox Signaling* (2018) doi:10.1089/ars.2017.6994.
65. Kyykallio, H. *et al.* The Density and Length of Filopodia Associate with the Activity of Hyaluronan Synthesis in Tumor Cells. *Cancers (Basel)* **12**, 1908 (2020).
66. Kuo, J. C.-H. & Paszek, M. J. Glycocalyx Curving the Membrane: Forces Emerging from the Cell Exterior. *Annu Rev Cell Dev Biol* **37**, 257–283 (2021).

SUPPLEMANTARY MATERIALS

Supplementary tables

Supp. Table 1. The details of protein labeling. Proteins specific information and necessary values for fluorescence dye volume calculations are listed.

	Amino acids	Predicted mass (kDa)	MW_p (kDa)	ME	V_d (µL)	Extinction coefficient ($M^{-1}cm^{-1}$)	C_p (mg/mL)	Degree of labeling
CD44	211	23.4	43	8	11	37275	~0.4	1.7
CD34	270	29	50	8	8.9	11835	~1	0.5
PODXL	405	43	165	8	6	15720	~1	1.1
PODXL2	468	52	110	8	5	35200	~0.8	1.3
Integrin	1745	192	260	8	1	176315	~1	3.1

Supplementary information

>sp|P16070|CD44_HUMAN CD44 antigen OS=Homo sapiens OX=9606 GN=CD44 PE=1 SV=3
MDKFWWHAAWGLCLVPLSLAQIDLNITCRFAGVFHVEKNGRYSISRTEAADLCKAF
NSTLPTMAQMEKALSIGFETCRYGFIEGHVVIPRIHPNSICAANNTGVYILTSNTSQY
DTYCFNASAPPEEDCTSVTDLPNAFDGPITITIVNRDGTRYVQKGEYRTNPEDIYPS
NPTDDDVSSGSSSERSSTSGGYIFYTFSTVHPIPDEDSPWITDSTDRIP

>NP_001020280.1 hematopoietic progenitor cell antigen CD34 isoform a precursor [Homo sapiens]
MLVRRGARAGPRMPRGWTALCLLSLLPSGFMSLDNNGTATPELPTQGTFSNVSTN
VSYQETTTPSTLGSTSLHPVSQHGNEATTNITETTVKFTSTSVITSVYGNTNSSVQS
QTSVISTVFTTPANVSTPETTLKPSLSPGNVSDLSTTSTSLATSPTKPYTSSSPILSDI
KAEIKCSGIREVKLTQGICLEQNKTSSCAEFKKDRGEGLARVLCGEEQADADAGAQ
VCSLLLAQSEVRPQCLLLVLANRTEISSKLQLMKKHQSDLKKLGILDFTEQDVASHQ
SYSQKT

>AAB61574.1 podocalyxin-like protein [Homo sapiens]
SPSPSPSPSPSQNATQTTTDSSNKTAPTPASSVTIMATDTAQQSTVPTSKANEILAS
VKATTLGVSSDSPGTTTLAQQVSGPVNTTVARGGGSGNPTTTIESPKSTKSADTTT
VATSTATAKPNTTSSQNGAEDTTNSGGKSSHSVTTDLTSTKAEHLTTPHPTSPLSP

RQPTLTHPVATPTSSGHDHLMKISSSSSTVAIPGYTFTSPGMTTTLPSSVISQRTQQ
TSSQMPASSTAPSSQETVQPTSPATALRTPTLPETMSSSPTAASTTHRYPKTPSPT
VAHESNWAKCEDLETQTQSEKQLVLNLTGNTLCAGGASDEKLISLICRAVKATFNPA
QDKCGIRLASVPGSQTVVVKEITIHTKLPAKDVYERLKDKWDELKEAGVSDMKLGD
QGPPEEAEDR

>sp|Q9NZ53.1|PDXL2_HUMAN RecName: Full=Podocalyxin-like protein 2; AltName: Full=Endoglycan; Flags: Precursor
GGAFLGACVAGSDEPGPEGLTSTSLLDLLLPTGLEPLDSEEPSETMGLGAGLGAPG
SGFPSEENEESRILQPPQYFWEEEEELNDSSLDLGPTADYVFPDLTEKAGSIEDTSQ
AQELPNLPSPLPKMNLVEPPWHMPPREEEEEEEEEEREKEEVEKQEEEEEEELLP
VNGSQEEAKPQVRDFSLTSSSQTPGATKSRHEDSGDQASSGVEVESSMGPSLLLP
SVTPTTVTPGDQDSTSQEAEATVLPAAGLGVEFEAPQEASEEATAGAAGLSGQHE
EVPALPSFPQTTAPSGAEHPDEDPLGSRTSASSPLAPGDMELTPSSATLGQEDLNQ
QLLEGQAAEAQSRIPWDSTQVICKDWSNLAGKNYIILNMTENIDCEVFRQHRGPQLL
ALVEEVLPRHGSGHHGAWHISLSKPSEKEQHLLMTLVGEQGVVPTQDVLSMLGDIR
RSLEEIGIQNYSTTSSCQARASQVRSDYGT

>sp|P08648|ITA5_HUMAN Integrin alpha-5 OS=Homo sapiens OX=9606 GN=ITGA5 PE=1 SV=2
MGSRTPESPLHAVQLRWGPRRRPPLLPLLLLLLPPPPRVGGFNLDAEAPAVLSGPP
GSFFGFSVEFYRPGTDGVSVLVGAPKANTSQPGVLQGGAVYLCPWGASPTQCTPI
EFDSKGSRLLESSLSSSEGEEPVEYKSLQWFGATVRAHGSSILACAPLYSWRTEKE
PLSDPVGTCYLSTDNFTRILEYAPCRSDFSWAAGQGYCQGGFSAEFTKTGRVVLG
GPGSYFWQGQILSATQEQIAESYYPEYLINLVQGQLQTRQASSIYDDSYLGYSVAVG
EFSGDDTEDFVAGVPKGNLTYGYVTILNGSDIRSLYNFSGEQMASYFGYAVAATDV
NGDGLDDLLVGAPLLMDRTPDGRPQEVGRVYVYLQHPAGIEPTPTLTLTGHDEFGR
FGSSLTPLGDLDQDGYNDVAIGAPFGGETQQGVVFVFPGGPGGLGSKPSQVLQPL
WAASHTPDFFGSALRGGRDLDGNGYPDLIVGSFGVDKAVVYRGRPIVSASASLTIF
PAMFNPEERSCSLEGNPVACINLSFCLNASGKHVADSIGFTVELQLDWQKQKGGVR
RALFLASRQATLTQTLLIQNGAREDCREMKIYLRNESEFRDKLSPIHIALNFSLDPQA
PVDSHGLRPALHYQSKSRIEDKAQILLDCGEDNICVPDLQLEVFGEQNHVYLGDKNA
LNLTFHAQNVGEGGAYEAELRVTAPPEAEYSGLVRHPGNFSSLSCDYFAVNQSRLL
VCDLGNPMKAGASLWGGLRFTVPHLRDTKKTIQFDFQILSKNLNNSQSDVVSFRLS
VEAQAQVTLNGVSKPEAVLFPVSDWHPRDQPQKEEDLGPAVHHVYELINQGPSSIS
QGVLELSCPQALEGQQLLYVTRVTGLNCTTNHPINPKGLELDPEGSLHHQQKREAP
SRSSASSGPQILKCPEAECFRLRCELGPLHQQESQSLQLHFRVWAKTFLQREHQPF
SLQCEAVYKALKMPYRILPRQLPQKERQVATAVQWTKAEGSY

>sp|P05556|ITB1_HUMAN Integrin beta-1 OS=Homo sapiens OX=9606 GN=ITGB1 PE=1 SV=2
MNLQPIFWIGLISSVCCVFAQTDENRCLKANAKSCGECIQAGPNCGWCTNSTFLQE
GMPTSARCDDLEALKKKGCPPDDIENPRGSKDIKKNKNVTNRSKGTAEKLKPEDIT
QIQPQQLVLRLRSGEPQTFTLKFKRAEDYPIDLYYLMDLSYSMKDDLENVKSLGTDL
MNEMRRITSDFRIGFGSFVEKTVMPYISTTPAKLRNPCTSEQNCTSPFSYKNVLSLT
NKGEVFNELVGKQRISGNLDSPEGGFDAIMQVAVCGSLIGWRNVTRLLVFSTDAGF
HFAGDGKLGGIVLPNDGQCHLENNMYTMSHYYDYPSIAHLVQKLSENNIQTIFAVTE

EFQPVYKELKNLIPKSAVGTLSANSSNVIQLIIDAYNSLSSEVILENGKLSEGVTISYKS
YCKNGVNGTGENGRKCSNISIGDEVQFEISITSNKCPKKDSDSFKIRPLGFTEEVEVI
LQYICECECQSEGIPESPKCHEGNGTFECGACRCNEGRVGRHCECSTDEVNSEDM
DAYCRKENSSEICSNNGECVCGQCVCRKRDNTNEIYSGKFCECDNFNCDRSNGLI
CGGNGVCKCRVCECNPNYTGSACDCSLDTSTCEASNGQICNGRGICECGVCKCT
DPKFQGQTCEMCQTCLGVCAEHKECVQCRAFNKGEKKDTCTQECSYFNITKVESR
DKLPQPVQPDPVSHCKEKDVDDCWFYFTYSVNGNNEVMVHVVENPECPTGPD

Supp. Info. 1. Amino acid sequences of his-tagged recombinant proteins. The amino acids sequences taken from UniProtKB or NCBI were listed for CD 44, CD34, PODXL, PODXL2, and Integrin, respectively.

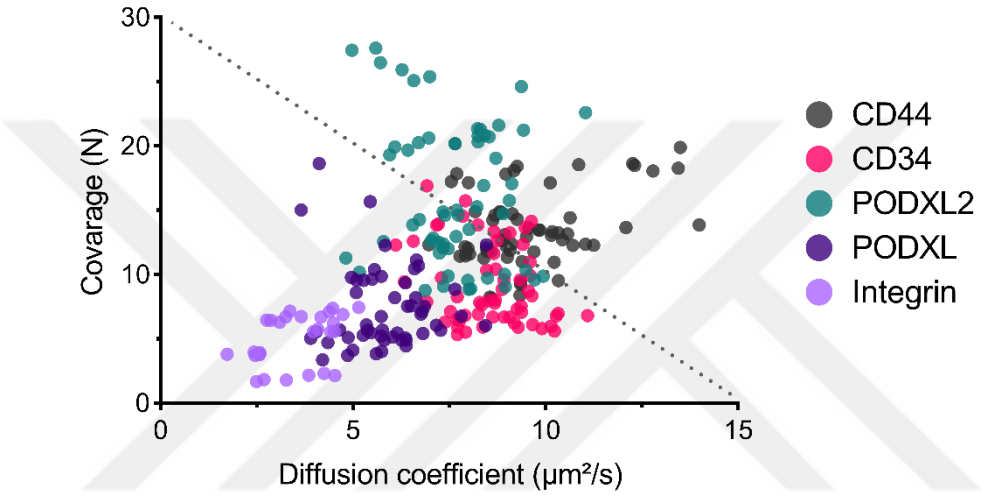

Supp. Info. 2. Number of molecules (coverage) vs. diffusion coefficient. The graph shows no notable inverse linear correlation of measured N and diffusion between different samples, confirming that there is no effect of N on observed differences in diffusion. Dotted line shows the hypothetical inverse correlation due to the effect of molecular crowding on diffusion.